Hindawi Publishing Corporation
Advances in Materials Science and Engineering
Volume 2014, Article ID 249174, 9 pages
http://dx.doi.org/10.1155/2014/249174

Research Article

A Study on the Effect of the Boron Potential on the Mechanical Properties of the Borided Layers Obtained by Boron Diffusion at the Surface of AISI 316L Steel

E. Hernández-Sánchez,[1] Y. M. Domínguez-Galicia,[1] C. Orozco-Álvarez,[1] R. Carrera-Espinoza,[2] H. Herrera-Hernández,[3] and J. C. Velázquez[4]

[1] *Instituto Politécnico Nacional, UPIBI, Avenida Acueducto s/n Barrio La Laguna Ticomán, 07340 México, DF, Mexico*
[2] *Instituto Tecnológico Superior de Poza Rica, Luis Donaldo Colosio Murrieta s/n, Arrollo del Maíz, 93230 Poza Rica, VER, Mexico*
[3] *Universidad Autónoma del Estado de México, Boulevard Universitario s/n, Predio San Javier, 54500 Atizapán de Zaragoza, MEX, Mexico*
[4] *Departamento de Ingeniería Química Industrial, IPN-ESIQIE, UPALM Edifício 7, 1er Piso, Zacatenco, 07738 México, DF, Mexico*

Correspondence should be addressed to E. Hernández-Sánchez; enriquehs266@yahoo.com.mx

Received 27 August 2014; Accepted 30 October 2014; Published 24 November 2014

Academic Editor: Ming-Xing Zhang

The effect of the boron potential on the thickness and the mechanical properties of borided layers was evaluated. The boron potential was established by means of the available atoms of boron contained in a control volume inside a cylinder. The cylinders were manufactured from AISI 316L steel, and the boriding treatment was performed using the powder pack technique at a temperature of 1273 K over an exposure time of 6 h. Four different internal diameters of the cylinders were evaluated (3.17, 4.76, 6.35, and 7.93 mm). The mechanical properties were evaluated using the Berkovich instrumented indentation technique. The results showed a clear influence of the boron potential on the mechanical properties of the layers. The hardness of the layers was stablished in the range of 16.22 to 21.16 GPa. Young's modulus values were stablished in the range of 255.96 to 341.37 GPa. Also the fracture toughness and brittleness of the layers reflected the influence of the boron potential supplied during the boriding process. Finally, the influence of the boron potential on the constant of parabolic growth (K) was also established as a function of the inner diameter of the cylinders.

1. Introduction

In the recent decades, the use in orthopedic applications of some metals, such as titanium alloys, cobalt alloys, and stainless steel, has been highly favored because of their good mechanical properties. Nevertheless, although these metals are specially designed to address corrosion, they tend to corrode when in contact with body fluids [1]. AISI 316L steel is considered a biomedical steel because its low carbon content does not cause intercrystalline corrosion. However, this type of steel may corrode inside the body under certain conditions [2].

The use of different processes of surface modification of AISI 316L steel has been presented as an alternative to minimize the corrosion when the material is in contact with living tissues [3]. Boriding is one of the most recently used processes to modify the surface of metallic materials. During the boriding process, atoms of boron are diffused into a metallic matrix to enhance the mechanical and chemical surface properties of the treated materials. The process takes place in solid, liquid, or gaseous media. The most commonly used method is pack boriding because it is cheaper and easier to perform than the others [4, 5]. During the pack boriding process, boron is generally provided from boron carbide (B_4C) or amorphous boron, an activator to deposit atomic boron at the surface substrate and a diluent. The process involves embedding the samples in the powder mixture and sealing them in a container. The container is then heated to the established temperature for the required amount of time according to the desired results [6]. By means of boron

Table 1: Available atoms of boron for the layer formation as a function of the inner diameter of the samples.

Sample number	Inner diameter of the samples (m)	Height of the samples (m)	Control volume (m^3)	$W_{mixture}$ (kg)	$W(B)_{mixture}$ (kg)	Available boron atoms
1	$3.17E-03$	$4.80E-03$	$3.788E-08$	$3.58E-05$	$2.58E-05$	$1.436E+21$
2	$4.76E-03$	$4.80E-03$	$8.542E-08$	$8.07E-05$	$5.82\,E-05$	$3.238E+21$
3	$6.35E-03$	$4.80E-03$	$1.520E-07$	$1.44E-04$	$1.04E-04$	$5.763E+21$
4	$7.93E-03$	$4.80E-03$	$2.371E-07$	$2.24E-04$	$1.61E-04$	$8.987E+21$

diffusion into steel alloys, it is expected to obtain iron borides with a single phase Fe_2B (containing approx. 8.83 wt.% B) or a double phase FeB/Fe_2B (with a FeB phase containing approx. 16.23 wt.% B) [7]. Different features, such as the chemical composition of the substrate, the boron potential supplied during the process, the temperature, and the treatment time, determine the resulting single or double phase layer. Likewise, the thickness of the boride layer is determined by the above-mentioned conditions [8].

This work evaluates the influence of the boron potential on the mechanical properties of borided layers. The samples were cylinders with different internal diameters, which allowed modification of the available amount of boron for the formation of borided layers. The main objective of the work was to establish the behavior of the mechanical properties of the borided layers when a preestablished amount of boron was supplied. The boron-area ratio is a direct function of the inner diameter of the samples; therefore, as the diameter is increased, the boron potential is also increased, and the mechanical properties of the layers are influenced by the increase.

2. Materials and Methods

2.1. Boriding Treatment. Cylindrical samples of AISI 316L steel with diameters of 25.4 mm and lengths of 50.8 mm were used to make four cylinders with different internal diameters (3.17, 4.76, 6.35, and 7.93 mm).

The chemical composition of the steel was 0.03% wt. C, 1.0% Si max, 2.0% wt. Mn max, 16/18% wt. Cr, 10/14% wt. Ni, 2/3% wt. Mo, 0.045% wt. P max, and 0.03% wt. S max, according to the distributor SISA, Mexico.

The cylinders were drilled to a depth of 48.8 mm to prevent the boriding agent from escaping the samples (see Figure 1).

The inside of the samples was filled with a boriding agent containing 5% wt. of B_4C as boron donor, 5% wt. of KBF_4 as activator, and 90% wt. of SiC as diluent, with a powder size of 50 μm [9]. The content of boron in the mixture allowed for the formation of the layers with a minimum amount of boriding mixture in the inner of the cylinders, which was called the Volume of Control. The weight of the mixture was registered to estimate the exact amount of boron atoms available for the layer formation (see Table 1) by considering the chemical reaction during the thermochemical treatment as follows:

$$B_4C + 3SiC + 3O_2 \xrightarrow[SiF_4]{BF_3} 4B + 2Si + SiO_2 + 4CO \quad (1)$$

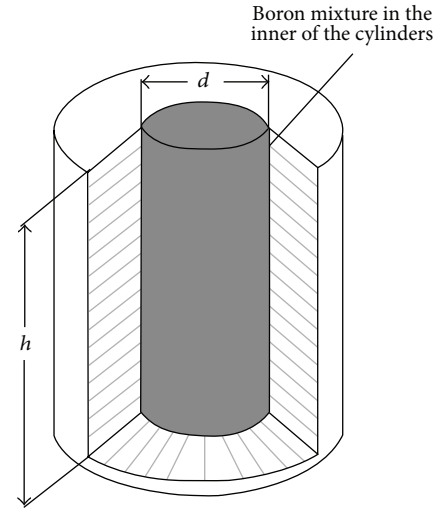

Figure 1: Schematic representation of the samples with the boron mixture.

In reaction (1), the KBF_4, which was added as an activator, melts at the boriding temperature and helps in sintering of the particles; thus, it is not a source of free boron [7]. In that sense, the fraction by weight of active boron in B_4C [$f(B)_{B_4C}$] can be obtained as follows:

$$f(B)_{B_4C} = \frac{4a_B}{[(4a_B) + a_C]}, \quad (2)$$

where a_B and a_C are the atomic weights of boron and carbon, respectively. The weight of the powder mixture W_{mix} (kg), in a specific volume, is obtained as

$$W_{mix} = \rho_{mix} V_{mix}. \quad (3)$$

Because the powder mixture contains 5% wt. of B_4C, the weight of boron available in the powder mixture $W(B)$ is obtained as

$$W(B)_{mix} = 0.05 W_{mix} f(B)_{B_4C}, \quad (4)$$

where W_{mix} is the weight of the mixture on the inside of the cylinders, $W(B)_{mix}$ is the weight of boron available in each sample, ρ_{mix} is the experimentally estimated density of the powder mixture (1240 kg/m^3), and V_{mix} is the volume on the inside of the samples. The available amount of boron atoms can be estimated by considering the atomic weight of boron.

The cylinders were collocated into a container of AISI 304 steel and embedded in SiC. A conventional furnace for

Table 2: Layer thickness as a function of the boron potential represented by the inner diameter of the samples at 1273 K and 6 h of exposure time.

Inner diameter of the samples	Layer thickness	
(mm)	FeB	Fe_2B
3.17	4.19 ± 1.85	26.30 ± 2.10
4.76	11.33 ± 1.65	31.38 ± 2.14
6.35	21.11 ± 3.14	37.67 ± 2.05
7.93	29.16 ± 2.84	40.40 ± 3.54

thermochemical treatments was used for the development of the process. The treatment conditions were established at 1273 K for 6 h. After the treatment was concluded, the container was removed from the furnace and was slowly cooled to room temperature.

The samples were prepared by standard metallographic techniques for microscopic examinations using GX51 Olympus equipment to determine the borided layer thickness. At least fifty measurements were performed from a fixed reference on different sections of borided samples; the mean thickness values of the FeB and Fe_2B phases are depicted in Table 2.

2.2. Kinetics of Growth. The kinetics of the growth of the layers is controlled by the boron diffusion, so the growth of borided layers occurs as a consequence of the boron diffusion in the perpendicular direction to the sample surface [10]. The growth of the FeB and Fe_2B phases obeys a parabolic law as follows:

$$x^2 = Kt, \tag{5}$$

where x is the layer thickness for both the FeB and Fe_2B layers, K is the constant of parabolic growth, and t is the treatment time.

As established previously, the boron potential is represented by the amount of boron mixture on the inside of the cylinders. In that sense, the layer thickness can be related with the boron potential by plotting the experimental layer thickness versus the inner diameter of the cylinders. The best fit of the resulting curve showed a tendency line in potential form as follows:

$$x = md^n. \tag{6}$$

Finally, relating (5) and (6), the constant of parabolic growth can be estimated as a function of the boron potential:

$$K = \frac{\left(md^n\right)^2}{t}, \tag{7}$$

where m and n are the resulting parameters of plotting x versus d in a potential form and d is the inner diameter of the cylinders, which represents the available boron potential for the boriding process.

2.3. Characterization. The presence of the FeB and Fe_2B phases was revealed by means of X-ray diffraction (XRD) using Bruker D8 FOCUS equipment with CuK_α radiation at $\lambda = 1.54$ Å.

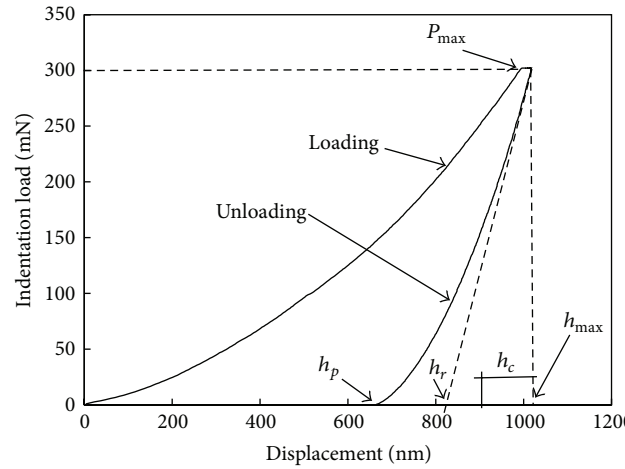

Figure 2: Schematic representation of a typical load versus indenter displacement data for an indentation test.

The mechanical properties in both phases, such as the hardness and Young's modulus, were evaluated by means of the instrumented indentation technique with the aid of a nanohardness tester (TTX-NHT, CSM Instruments) using a Berkovich indenter and following the methodology established by Oliver and Pharr [11]. According with Oliver and Pharr method, in nanoindentation, the depth of penetration of a diamond indenter is measured along with the prescribed load. The resulting load-displacement response typically shows an elastic-plastic loading followed by an elastic unloading (see Figure 2). The elastic equations of contact are then used in conjunction with the unloading data to determine Young's modulus and hardness of the specimen material as follow:

$$H = \frac{P}{A_c},$$
$$E = \frac{1 - \nu_s^2}{\left(1/E_r\right) - \left(\left(1 - \nu_i^2\right)/E_i\right)}, \tag{8}$$
$$E_r = \frac{\sqrt{\pi}S}{2\beta\sqrt{A_c\left(h_c\right)}},$$

where H is the hardness of the specimen, P is the applied load, A_c is the contact area at peak load ($24.49\,h_c^2$), h_c is the experimentally measured contact indentation depth, 24.49 is a constant related with the geometry of the indenter, E is Young's modulus, ν_s is Poisson's ratio of the sample (0.3), ν_i is Poisson's ratio of the indenter (0.07), E_i is Young's modulus of the indenter (1141 GPa), E_r is a reduced modulus of the indentation contact, and S is the stiffness of the sample.

A set of ten indentations was realized in the compact zone of both phases FeB and Fe_2B. The distance between indentation prints was established by following the limits of the ISO instrumented indentation standards (ISO 14577-1-2002) to avoid interaction between the stresses field of the

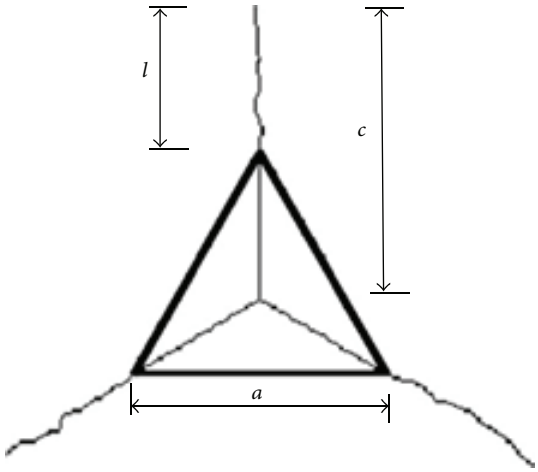

Figure 3: Schematic representation of the crack length formed at the corners of the Berkovich nanoindentation print.

indentations [12]. The indentation load was established at 300 mN because the generation of cracks was evident with that load.

The fracture toughness (K_c) in both phases was evaluated based on the condition that when $c/a \geq 2.5$, the exhibited cracking regime is considered radial media. This condition was observed in the FeB phase, so that the fracture toughness in that phase was evaluated by applying a model proposed by Anstis et al. [13] as follows:

$$K_c = 0.016\left(\frac{E}{H}\right)^{1/2}\frac{P}{c^{3/2}}, \tag{9}$$

where 0.016 is a constant related to the properties of the Berkovich indenter, E is Young's modulus, H is the hardness at the respective phase of the layer, P is the applied load, and c is the length of the crack measured from the center of the indentation print (see Figure 3).

On the other hand, the Palmqvist cracking regime was observed in the Fe_2B phase because the relation $(1/a)^{-1/2}$ tended to be near 0.68, which was a condition reported by Laugier [14]. In addition, the cracking process in the Fe_2B phase satisfied the condition of $0.25 \leq l/a \leq 2.5$, proposed for the Palmqvist regime. Therefore, the fracture toughness at the Fe_2B phase was evaluated by means of a model proposed by Laugier, as follows:

$$K_c = K^p\left(\frac{l}{a}\right)^{-1/2}\left(\frac{E}{H}\right)^{2/3}\frac{P}{c^{3/2}}, \tag{10}$$

where K^p is a constant that is numerically determined (0.015), a is the half diagonal length, and l is the crack length measured from the corner of the indentation print (see Figure 3).

The crack length was measured with the aid of a scanning electron microscope (SEM) (JEOL, JSM-7401) as described in Figure 3.

Finally, the behavior of the brittleness (B) of the FeB and Fe_2B phases was evaluated by means of a model proposed by J. B. Quinn and G. D. Quinn [15]; the influence of the boron potential on the brittleness of the layers is related on the fracture process and the deformation process as follows:

$$B = \frac{HE}{K_c^2}. \tag{11}$$

According to the Quinn model, the brittleness of the layers is highly related with the fracture process because the brittleness values are highly sensitive to small variations in the fracture toughness values.

3. Results and Discussion

3.1. Microstructure. Optical examination of the surface of AISI 316L borided steels revealed the presence of two phases of borides in samples 2, 3, and 4, which were assumed to be FeB/Fe_2B because of the difference in the contrast of the interface (Figure 4).

This assumption was corroborated by the XRD analysis, as shown in Figure 5, in which the outermost phase is FeB and the inner phase is Fe_2B. In sample number 1, only small isolated portions of FeB phase were generated, so it is possible to assume that the amount of boron provided in that sample was enough for the formation of a monophasic Fe_2B layer.

Likewise, in samples 2, 3, and 4, it is possible to observe how the FeB phase increased in thickness as the boron potential was increased, even though the treatment conditions (time and temperature) were constant during the process. This behavior suggests that the thickness of the FeB phase on the borided layers can be controlled by controlling the boron potential during the boriding treatment, which represents a great advantage because the FeB phase is considered as an undesirable subproduct of the boriding process [16].

In comparison with carbon steels, where the resulting layers have saw-toothed shape, the morphology of the growth interfaces of the borided layers in the AISI 316L steel was flat (see Figure 4). This morphology can be explained because the high content of alloying elements in the substrate tends to react with boron and forms different compounds, such as CrB, Cr_2B, and Ni_3B [17, 18]. Figure 6 shows the best fit of the graph of the layer thickness versus the inner diameter of the samples and the values m and n for both phases are summarized in Table 3.

The resulting equations for the evaluation of the constant of parabolic growth, according to (7), are as follows:

$$K_{\mathrm{FeB}} = \frac{\left[(1.3493E-07)\,d^{2.1468}\right]^2}{21600},$$
$$K_{\mathrm{Fe_2B}} = \frac{\left(0.5259d^{0.4849}\right)^2}{21600}. \tag{12}$$

In Figure 6, the difference in the inner diameter of the samples has a strong influence on the thickness of the layers, even when the boron potential in the smallest cylinder (sample 1) was sufficient for the formation of the layers. Such behavior can be explained by the fact that the atoms of boron are confined in a cylinder so that the diffusion process could

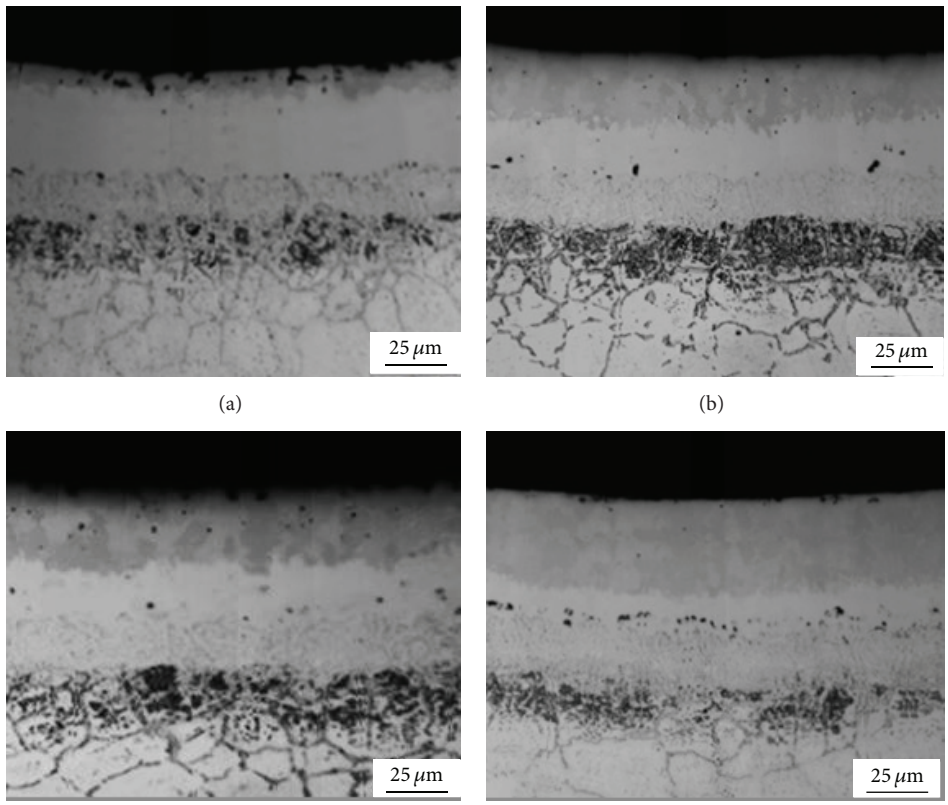

Figure 4: Optical view of the cross-section of the AISI 316L steel borided at a temperature of 1273 K with 6 h of exposure with an inner diameter of (a) 3.17, (b) 4.76, (c) 6.35, and (d) 7.93 mm.

Table 3: Behavior of the constant of parabolic growth of the FeB and Fe_2B phases as a function of the boron potential represented by the inner diameter of the samples.

Sample number	Parameters of the plot x versus d				Constant of parabolic growth (K) (m^2s^{-1})	
	FeB		Fe_2B			
	m	n	m	n	FeB	Fe_2B
1	$1.35E-07$	2.1468	0.5259	0.4849	$9.08577E-16$	$3.18185E-14$
2					$5.2046E-15$	$4.7195E-14$
3					$1.79392E-14$	$6.24141E-14$
4					$4.65729E-14$	$7.74226E-14$

be more efficient because of the total amount of boron atoms interacting with the surface of the sample. Additionally, the amount of available atoms of boron for the layer formation increases proportionally to the inner diameter of the samples, as shown in Table 1. The amount of atoms of boron mentioned above could be evaluated accurately because the samples were cylinders with a specific volume, which is called the "Volume of Control." Likewise, according to the reaction that occurs during the boriding process, the only source of boron available for the layers formation is B_4C [7], which represents 5% wt. of total mixture on the inside of the samples. Conversely, in Figure 1, the total area to cover with borided layers is given by the relation $A = \pi dh$, where A is the area to cover with the borided layer, d is the inner diameter of the cylinders, and h is the height of the cylinders. According to the values summarized in Table 1, the available amount of atoms of boron for the formation of the layers increases as the inner diameter of the cylinders is increased. This condition suggests that the layer thickness will increase by increasing the inner diameter of the cylinders. The experimental results confirmed this hypothesis because the thickness of the layer was increased with the increase in the inner diameter of the samples, as shown in Figures 4 and 6.

Figure 7 shows the behavior of the constant of parabolic growth (K) as a function of the inner diameter of the samples.

The values of (K) in both phases FeB and Fe_2B increase as the inner diameter of the samples increases, which indicates a controlled diffusion process. The results shown in Table 2

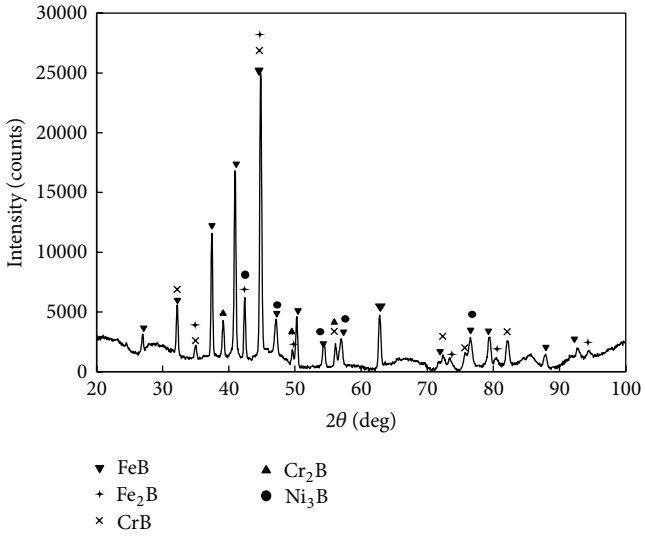

Figure 5: XRD pattern of AISI 316L steel borided for 6 h at a temperature of 1273 K and an inner diameter of the sample of the 6.35 mm (sample 3).

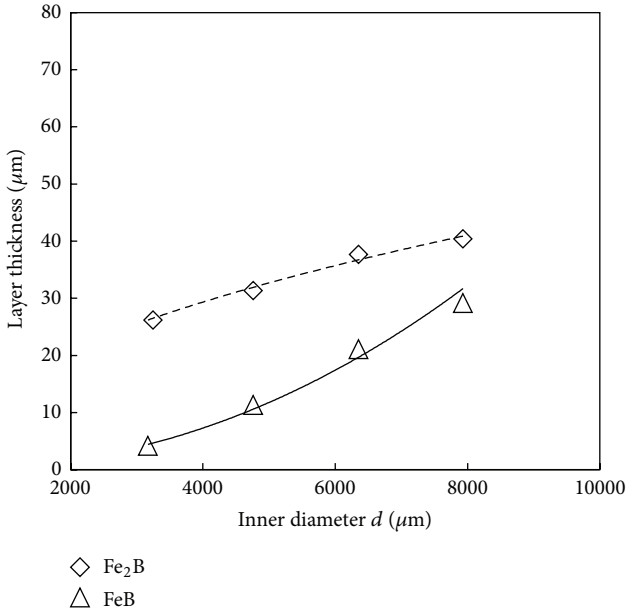

Figure 6: Behavior of the layer thickness as a function of the boron potential represented by the inner diameter of the samples.

suggest that the thickness of the FeB phase can be controlled by controlling the boron potential during the thermochemical process.

3.2. Mechanical Characterization. The hardness behavior of the FeB and Fe_2B phases as a function of the inner diameter of the samples is shown in Figure 8(a) and summarized in Table 4.

According to the graph, the hardness of the layers increased as the boron potential was increased. This behavior can be explained because the sample with the lowest boron

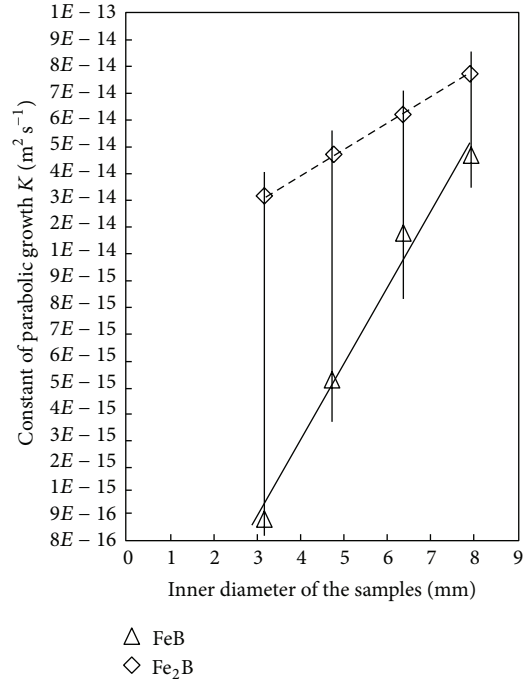

Figure 7: Constant of parabolic growth as a function of the boron potential represented by the inner diameter of the samples.

potential (sample 1) did not exhibit a layer with the FeB phase, whereas the sample with the highest boron potential (sample 4) exhibited the biggest FeB phase (see Table 2). The greatest thickness of FeB phase results as a consequence of the increment in the flux of boron due to the increased inner diameter of the samples (Figure 9).

Likewise, the FeB phase is harder than the Fe_2B phase, so it is expected that the layer with the thickest FeB phase has the highest hardness as well. Nevertheless, the formation of a monophasic layer (Fe_2B) is more desirable than that of a biphasic layer with FeB and Fe_2B due to the difference in the thermal expansion coefficient between both phases [19, 20]. This behavior highlights the importance of controlling the boron potential during the boriding process in order to control the mechanical properties of the achieved layers.

Young's modulus behavior was established as a function of the boron potential, and its values are summarized in Table 4. According to the results, the boron potential provided during the process has a strong influence on Young's modulus of the layers because, as the boron potential increases, the hardness of the layers increases and Young's modulus is directly related to the hardness of the layers [21]. In addition, Young's modulus of the FeB phase remained practically constant, whereas, in the Fe_2B phase, it increased drastically as the boron potential was increased (see Figure 8(b)). The increase in Young's modulus values in the Fe_2B phase generates an increase in the brittleness of the layers [13–15]; therefore, by controlling the boron potential during the process, it may be possible to control the brittleness of the layers.

The fracture toughness of the borided layers was evaluated by applying two different models as a function of the

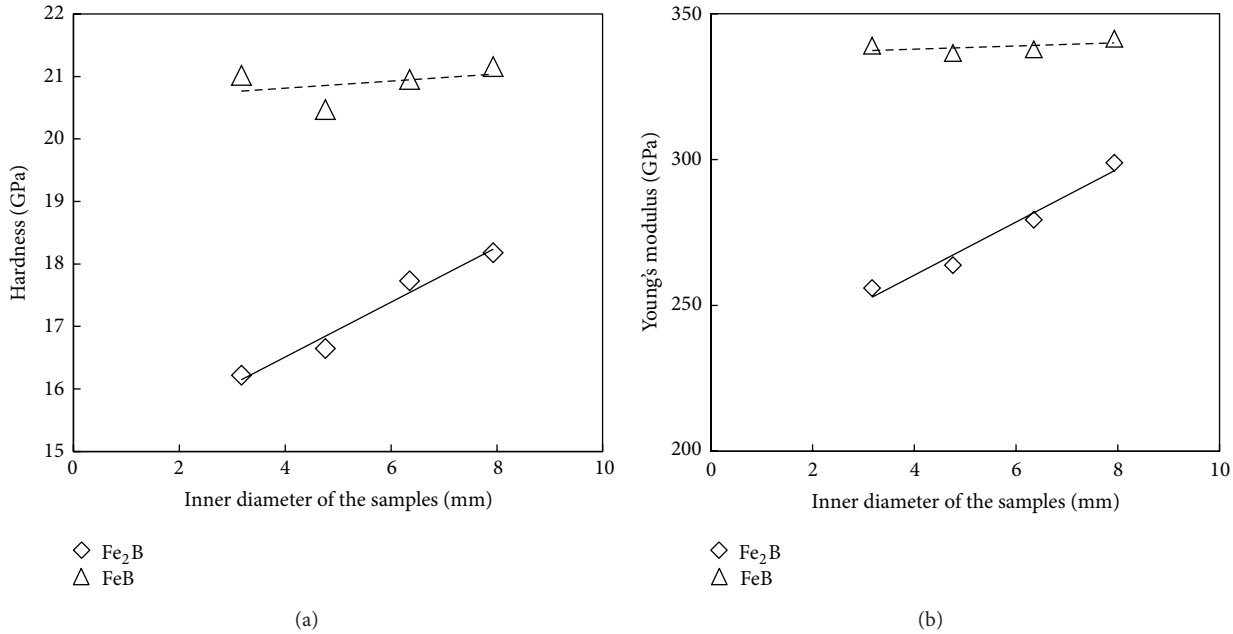

Figure 8: Behavior of the (a) hardness and (b) Young's modulus of the FeB and Fe_2B phases as a function of the boron potential represented by the inner diameter of the samples.

Table 4: Behavior of the hardness and Young's modulus of the FeB and Fe_2B phases as a function of the boron potential represented by the inner diameter of the samples.

Sample number	Inner diameter of the samples (mm)	HV (GPa)		E (GPa)	
		FeB	Fe_2B	FeB	Fe_2B
1	3.17	21.02 ± 2.7	16.22 ± 3.7	338.98 ± 24.4	255.96 ± 22.8
2	4.76	20.47 ± 1.7	16.65 ± 3.1	336.46 ± 23.2	263.76 ± 18.8
3	6.35	20.95 ± 3.4	17.73 ± 3.4	337.78 ± 19.9	279.38 ± 24.7
4	7.93	21.16 ± 2.6	18.18 ± 2.9	341.37 ± 22.3	298.92 ± 27.9

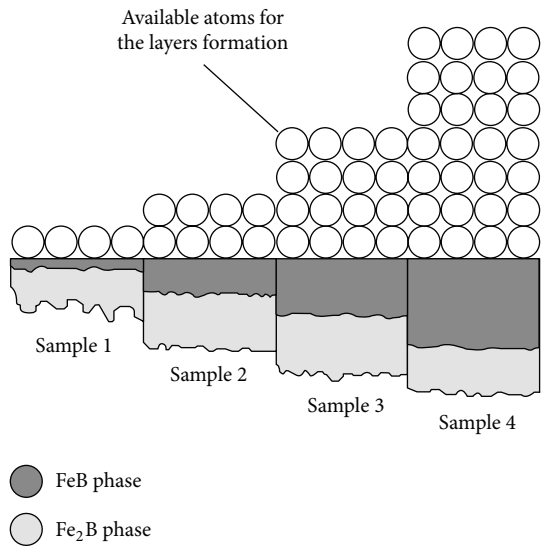

Figure 9: Schematic representation of the available boron atoms for the layers formation as a function of the boron potential represented by the inner diameter of the samples.

Table 5: K_c values for the FeB and Fe_2B phases as a function of the boron potential represented by the inner diameter of the samples.

Sample number	Inner diameter of the samples (mm)	K_c (MPa $m^{1/2}$)	
		FeB (9)	Fe_2B (10)
1	3.17	—	3.03 ± 0.37
2	4.76	1.59 ± 0.19	2.81 ± 0.19
3	6.35	1.32 ± 0.27	2.53 ± 0.27
4	7.93	1.23 ± 0.23	2.22 ± 0.30

cracking regime exhibited by each phase (radial media for FeB and Palmqvist for Fe_2B). The fracture toughness behavior as a function of the inner diameter of the samples is shown in Figure 10 and summarized in Table 5.

The results indicate that the layers formed in the presence of the lowest content of boron (sample 1) were less susceptible to fracture than those with the highest boron content (sample 4). Likewise, the layer with the thickest FeB phase is also more apt to fracture. This behavior highlights the influence of the hardness in the fracture toughness values because, as

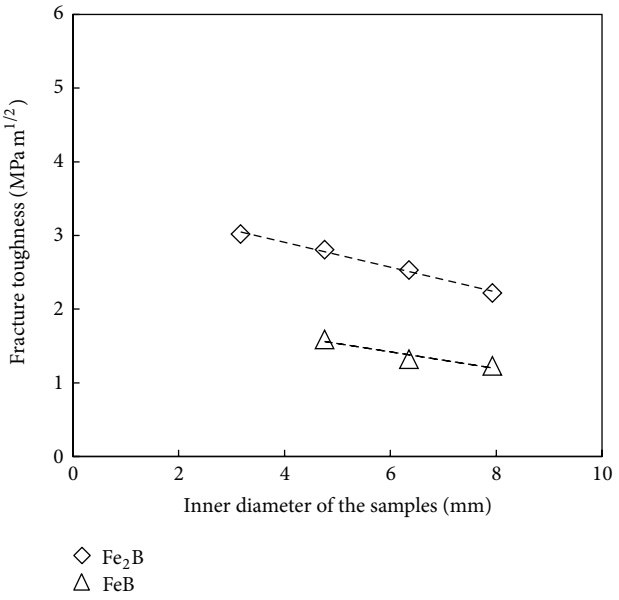

Figure 10: Behavior of the fracture toughness of both FeB and Fe_2B phases as a function of the boron potential represented by the inner diameter of the samples.

Table 6: Brittleness values of the FeB and Fe_2B phases as a function of the boron potential represented by the inner diameter of the samples.

Sample number	Inner diameter of the samples (mm)	Brittleness (m^{-1})	
		FeB (9)	Fe_2B (10)
1	3.17	—	455.15
2	4.76	2724.31	556.19
3	6.35	4061.35	773.87
4	7.93	4774.57	1102.66

the hardness increases, the fracture toughness also increases. The fracture toughness of the borided layers was evaluated with a constant load of 300 mN, so that it was not necessary to consider the load-independent hardness values to eliminate the effect of the apparent hardness into the fracture toughness equations [22]. Likewise, the applied models only consider the cracks generated in the corners of the indentation prints. Finally, the brittleness of the FeB and Fe_2B phases was evaluated as a function of the different inner diameters of the samples, in order to establish the influence of the boron potential on the brittleness of the layers. According to the results depicted in Figure 11 and summarized in Table 6, the FeB phase exhibited higher brittleness than the Fe_2B.

This difference in the brittleness values of both phases is because, according to J. B. Quinn and G. D. Quinn model [15], the brittleness of the layer is highly dependent on the fracture toughness, so that as the fracture toughness is increased, the brittleness of the layers decreases. Likewise, the brittleness of the layer tended to increase as the boron potential was increased, which confirms the assumption that the mechanical properties are strongly related to the boron potential supplied during the boriding treatment.

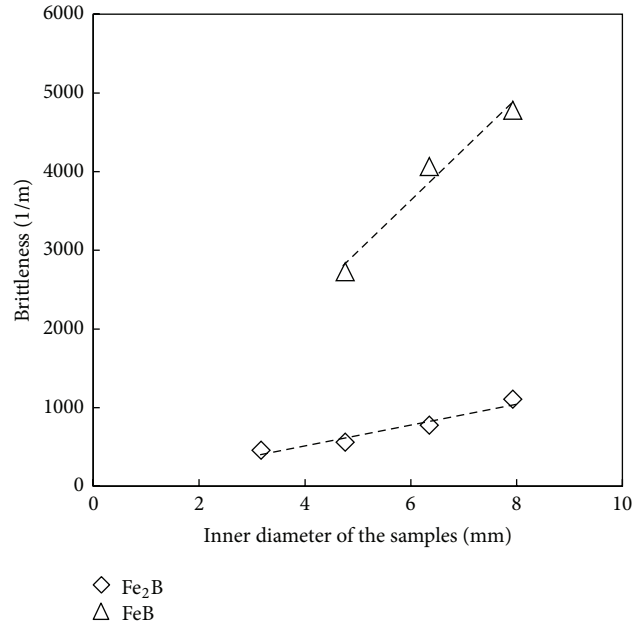

Figure 11: Behavior of the brittleness of the layers as a function of the boron potential represented by the inner diameter of the samples.

4. Conclusions

The following conclusions can be derived from the present study.

(a) The boron potential can be established as a function of the inner diameter of a cylinder, where the variation in the boron potential is a result of varying the inner diameter of the cylinder.

(b) The layer thickness was increased by increasing the boron potential, which is reflected in the values of the constant of parabolic growth.

(c) The hardness of the FeB phase was practically constant and was established in a range of 20.47 to 21.16 GPa, whereas the hardness of the Fe_2B phase increased in the range of 16.22 to 18.18 GPa as the boron potential was increased. This behavior is related to the increase in the FeB thickness.

(d) The fracture toughness was established in the range of 1.23 to 1.59 MPa $m^{1/2}$ for the FeB phase and in the range of 2.21 to 3.03 MPa $m^{1/2}$ for the Fe_2B phase. The decrease in the fracture toughness values reflects the influence of the boron potential on the mechanical properties of the layers during the process.

(e) The influence of the boron potential on the borided layers is clearly reflected in the thickness of the FeB phase because the FeB phase increased as the boron potential was increased, which suggests that it is possible to achieve a monophasic Fe_2B layer by controlling the boron potential during the process.

Conflict of Interests

The authors declare that there is no conflict of interests regarding the publication of this paper.

Acknowledgments

The authors wish to thank the Nanosciences Center and Micro-Nano Technologies of the Instituto Politécnico Nacional, for their cooperation. They would like to thank Dr. F. Caleyo Cereijo of the Instituto Politécnico Nacional-ESIQIE for his cooperation. Additionally, they would like to thank the Surface Engineering Group of the Instituto Politécnico Nacional-ESIME for its collaboration in the development of this work.

References

[1] H.-G. Neumann, U. Beck, M. Drawe, and J. Steinbach, "Multilayer systems for corrosion protection of stainless steel implants," *Surface and Coatings Technology*, vol. 98, no. 1–3, pp. 1157–1161, 1998.

[2] I. Özbek, B. A. Konduk, C. Bindal, and A. H. Ucisik, "Characterization of borided AISI 316L stainless steel implant," *Vacuum*, vol. 65, no. 3-4, pp. 521–525, 2002.

[3] I. Gurrappa, "Development of appropriate thickness ceramic coatings on 316 L stainless steel for biomedical applications," *Surface and Coatings Technology*, vol. 161, pp. 70–78, 2002.

[4] O. Allaoui, N. Bouaouadja, and G. Saindernan, "Characterization of boronized layers on a XC38 steel," *Surface and Coatings Technology*, vol. 201, no. 6, pp. 3475–3482, 2006.

[5] M. Keddam and S. M. Chentouf, "A diffusion model for describing the bilayer growth (FeB/Fe_2B) during the iron powder-pack boriding," *Applied Surface Science*, vol. 252, no. 2, pp. 393–399, 2005.

[6] M. Graf von Matuschka, *Boronizing*, Carl Hanser, Munich, Germany, 1st edition, 1980.

[7] V. Jain and G. Sundararajan, "Influence of the pack thickness of the boronizing mixture on the boriding of steel," *Surface and Coatings Technology*, vol. 149, no. 1, pp. 21–26, 2002.

[8] I. Campos, O. Bautista, G. Ramírez, M. Islas, J. De La Parra, and L. Zúñiga, "Effect of boron paste thickness on the growth kinetics of Fe_2B boride layers during the boriding process," *Applied Surface Science*, vol. 243, no. 1–4, pp. 429–436, 2005.

[9] G. Wahl, "Durferrit—technical information," Tech. Rep. VDI-Z117, 1975.

[10] O. Ozdemir, M. A. Omar, M. Usta, S. Zeytin, C. Bindal, and A. H. Ucisik, "An investigation on boriding kinetics of AISI 316 stainless steel," *Vacuum*, vol. 83, no. 1, pp. 175–179, 2008.

[11] W. C. Oliver and G. M. Pharr, "Improved technique for determining hardness and elastic modulus using load and displacement sensing indentation experiments," *Journal of Materials Research*, vol. 7, no. 6, pp. 1564–1580, 1992.

[12] B. R. Lawn, A. G. Evans, and D. B. Marshall, "Elastic/plastic indentation damage in ceramics: the median/radial crack system," *Journal of the American Ceramic Society*, vol. 63, no. 9-10, pp. 574–581, 1980.

[13] G. R. Anstis, P. Chantikul, B. R. Lawn, and D. B. Marshall, "A critical evaluation of indentation techniques for measuring fracture toughness: I, direct crack measurements," *Journal of the American Ceramic Society*, vol. 64, no. 9, pp. 533–538, 1981.

[14] M. T. Laugier, "New formula for indentation toughness in ceramics," *Journal of Materials Science Letters*, vol. 6, pp. 355–356, 1987.

[15] J. B. Quinn and G. D. Quinn, "Indentation brittleness of ceramics: a fresh approach," *Journal of Materials Science*, vol. 32, no. 16, pp. 4331–4346, 1997.

[16] U. Sen and S. Sen, "The fracture toughness of borides formed on boronized cold work tool steels," *Materials Characterization*, vol. 50, no. 4-5, pp. 261–267, 2003.

[17] G. Palombarini and M. Carbucicchio, "On the morphology of thermochemically produced Fe_2B/Fe interfaces," *Journal of Materials Science Letters*, vol. 3, no. 9, pp. 791–794, 1984.

[18] I. Campos-Silva, M. Ortiz-Domínguez, O. Bravo-Bárcenas et al., "Formation and kinetics of FeB/Fe_2B layers and diffusion zone at the surface of AISI 316 borided steels," *Surface and Coatings Technology*, vol. 205, no. 2, pp. 403–412, 2010.

[19] L. G. Yu, X. J. Chen, K. A. Khor, and G. Sundararajan, "FeB/Fe2B phase transformation during SPS pack-boriding: boride layer growth kinetics," *Acta Materialia*, vol. 53, no. 8, pp. 2361–2368, 2005.

[20] A. K. Sinha, *ASM Handbook*, vol. 4, ASM International, Materials Park, Ohio, USA, 1991.

[21] I. Campos-Silva, N. López-Perrusquia, E. Hernández-Sánchez, M. Ortíz-Domínguez, D. Bravo-Bárcenas, and J. Martínez-Trinidad, "Anisotropy of boride layers: effect on the mechanical properties of AISI 4140 borided steels," *Defect and Diffusion Forum*, vol. 297–301, pp. 142–147, 2010.

[22] F. Sergejev and M. Antonov, "Comparative study on indentation fracture toughness measurements of cemented carbides," *Proceedings of the Estonian Academy of Sciences Engineering*, vol. 12, no. 4, pp. 388–398, 2006.